Performance Evaluation of Free Hole Transport Layer CsPbI3 Perovskite Solar cells

Hadeer AbdElAziz (hadier.abdelaziz@gmail.com)
cpc: cooperative petroleum company https://orcid.org/0000-0002-4386-2722

Research Article

Keywords: SCAPS, CsPbI3, Perovskite solar cells, Nano

Posted Date: April 25th, 2022

DOI: https://doi.org/10.21203/rs.3.rs-1556737/v1

Performance Evaluation of Free Hole Transport Layer $CsPbI_3$ Perovskite Solar cells

Hadeer H. AbdelAziz[1]

[1] Research and development department, Coop Company, Cairo, Egypt

E-mail: h.hesham@cpc.com.eg

Abstract

Full inorganic cesium lead iodide ($CsPbI_3$) HTL free transport layer is investigated and simulated using SCAPS. The aim of the study is to investigate the optimum performance of the device structure. Using DFT study, the optical refractive index and reflectivity of $CsPbI_3$ are calculated. Further investigation of the device performance with changing parameters like metal back contact, absorber thickness, acceptor density, and defect density. The solar cell device has the optimum performance with Selenium as a back contact. The solar cell device structure of (FTO/ZnO/$CsPbI_3$/Se) with Voc of 1.34 V, Jsc of 19.75 mA/cm^2, an FF of 87.5%, and PCE of 23.25% are acquired for the proposed HTL-free $CsPbI_3$-based PSC. The simulation study will be a guide in fabricating low cost highly efficient HTL free inorganic $CsPbI_3$ solar cells.

Keywords: SCAPS, $CsPbI_3$, Perovskite solar cells, Nano

1. Introduction

The supply of energy is one of the most targeted goals for sustainable development. The traditional sources of energy are based on burning fuels which results in harmful carbon gases evolution and global warming climate change. Renewable energy like solar energy is considered an effective energy source candidate. Converting solar energy to electricity, solar cell device is a such condensed research area. Perovskites are emerging materials in photovoltaic applications. Perovskite materials have the ability to capture solar light efficiently and their bandgap can be tuned [1–3]. The first time used perovskite material is inorganic-organic metal halide $CH_3NH_3PbI_3$ and $CH_3NH_3PbBr_3$ as a photosensitizer [4]. After that, metal halide perovskites are used in solar cell devices. The problem with organic-metal halide-based perovskite materials are the organic compound like $CH_3NH_3^+$ $(MA)^+$or $HC(NH_2)_2$ $(FA)^+$ which are degradable and this affects the stability of the cell [5,6]. The organic cation can be replaced by metal cations like Cs^+ or Rb^+ [7,8]. Recently, caesium lead tri-iodide $CsPbI_3$ material received a lot of attention. $CsPbI_3$ is a perovskite material with bandgap of ~1.7 eV [9]. The material is extensively studied theoretically and experimentally [9–15]. For the solar device scale, the conventional planar perovskite solar cell is composed of Fan TO layer followed by ETL, the main perovskite layer, and an HTL layer. The commercialization of PSC faces many obstacles. One of these is the high expensive most used conventional spiro-OMeTAD HTL material. Spiro-OMeTAD is a highly expensive material for solar cell devices. Also, Spiro-OMeTAD material is an organic degradable material and affects the stability of the device [16]. Regular TiO_2 ETL material has the problem of decreasing solar cell device stability, as TiO_2 is sensitive to ultra-violet light of the spectrum and high annealing temperature[17,18]. The formation of $CsPbI_3$ on the TiO_2 ETL layer is at a temperature of 190° C [18]. On the other hand, ZnO material has many advantages as an ETL material for $CsPbI_3$. ZnO has high electron mobility, a good lattice match with $CsPbI_3$, and allows for low-temperature preparation with $CsPbI_3$ at 120° C [19]. A carbon-based perovskite solar cell offers a cost-effective solution for the PSC. The C-PSC is a solar cell structure that will be FTO/ETL/Perovskite/Carbon.

In this study**,** a DFT study is carried out on $CsPbI_3$ cubic perovskite. The aim of the DFT study is to explore the additional optical and electronic properties of the material. A theoretical investigation, for the first time, of the optical refractive index, reflectivity, and loss function is done. $CsPbI_3$ hole-free based perovskite solar cell device is optimized by numerical simulation

using SCAPS-1D. The ETL material is ZnO. The impact of metal back contact work function, $CsPbI_3$ thickness, concentration doping, and defect density on PCE are studied. The results offer a guide for designing high-performance HTL-free based inorganic $CsPbI_3$ perovskite solar cells.

2. Computational study

DFT study is carried out on cubic perovskite $CsPbI_3$ (Pm-3m, 221) structure. The study aims to calculate the band structure, density of states, and the optical properties like (refractive index, reflectivity, and absorption spectrum versus solar spectrum). Cambridge Sequential Total Energy Package (CASTEP)[20] was used in the DFT study. The exchange correlation between electrons for the $CsPbI_3$ cubic structure is studied by the Generalized Gradient Approximation – Perdew Burke Ernzerhof (GGA-PBE) functional [21]. GGA-PBE is a time saving function however it estimated the band gap of $CsPbI_3$ close to experimental. Ultra-soft pseudopotential is used with a Brillion k-point set of 3×3×3 and cut-off energy of 700 eV. To relax the CsPbI3 structure, the Boryden fletcher Goldfarb shanno (BFGS) algorithm is used. A medium convergence tolerance was used with an energy of 2×10^{-5} eV/atom, the maximum force of 0.05 eV/A° and the maximum displacement of 0.002 A°. The optimization steps were set to not exceed 1000 iterations. The self-consistent field (SCF) tolerance is set to 2×10^{-6} eV/atom.

Table 1 shows the calculated values of lattice constant, bandgap and real refractive index of $CsPbI_3$ material using GGA-PBE functional versus experimental values. The calculated and experimental values of the lattice constant of $CsPbI_3$ are 6.3 A and 6.4 A, respectively. The calculated band gap of $CsPbI_3$ equals to 1.6 while the experimental equals to1.67. The real part of the refractive index n at wavelength of 435 nm (2 calculated and 2.46 for experimental measures). The calculated values with GGA-PBE are with agreement with experimental one.

Table 1 Calculated lattice constant, bandgap, and real part of refractive index parameters of cubic CsPbI3 (Pm-3m, 221) perovskite using GGA-PBE functional versus experimental values

	GGA-PBE	Experimental
Lattice constant	6.3	6.4[22]
Bandgap (eV)	1.6	1.67[23]
Real refractive index n at 435 nm	2	2.46[23]

Figure 1 (a) shows the calculated band structure of $CsPbI_3$. The material is a direct bandgap semiconductor with calculated bandgap value of of 1.6 eV using GGA-PBE functional. The total density of states (DOS) and partial density of states (PDOS) calculations are shown in figure 1 (b). It is shown that, the valence band dominance is by p states from Pb-I states. The dominance in the conduction band s states for Cs and p states for Pb-I states.

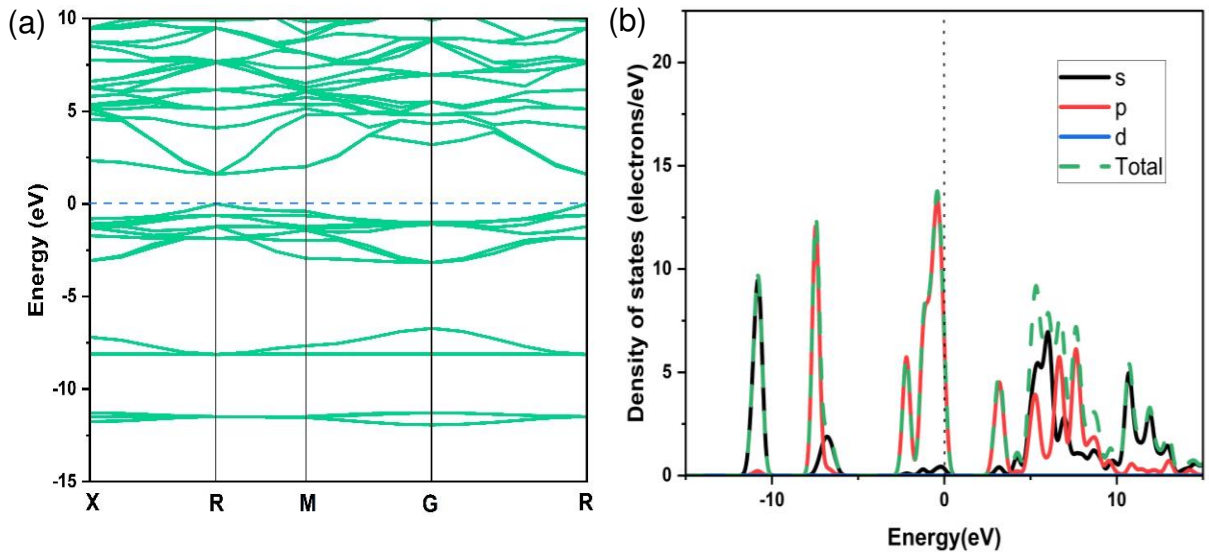

Figure 1 The calculation of $CsPbI_3$ (Pm-3m, 221) cubic perovskite (a) band structure (b) DOS using GGA-PBE functional

Figure2 (a) shows the optical refractive index as a function of wavelength (real *n* and imaginary *k*). It is shown that, the $CsPbI_3$ perovskite material has relatively low values of refractive index compared to other semiconductor materials, like Si and GaAs [24,25]. These lower values of n are advantageous for the device scale fabrication by avoiding losing light by reflection. The k (extinction coefficient) values of $CsPbI_3$ material is relatively higher than those of the organic metal halide perovskite such as $CH_3NH_3PbBr_3$ in the visible range of light [26,27]. This means that, the $CsPbI_3$ is relatively opaque to light in this range of light.

Figure 2 (b) shows the reflectivity versus wavelength for the $CsPbI_3$ perovskites. The reflectivity is used to study the surface properties of a material, which is equal to the ratio of the reflection to the incident power. These materials show low reflectivity in the first half of the spectrum, but for lambda > 550 nm the reflectivity increases.

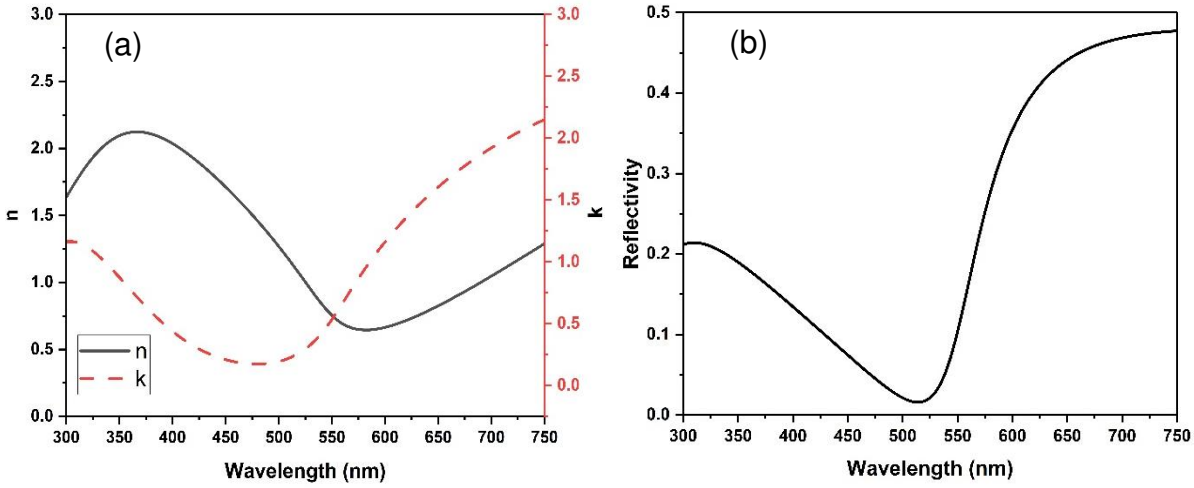

Figure 2 The optical properties of $CsPbI_3$ (a) real and imaginary refractive index, (b) reflectivity

2.1 Device structure numerical simulation study

All simulations are done using SCAPS-1D simulator [28]. As shown in Figure 3(a) $CsPbI_3$ HTL-free PSC consists of FTO/ETL/$CsPbI_3$/HTL/Carbon. The bandgap alignment between $CsPbI_3$ and ZnO is shown in Figure 3(b) The physical parameters of used materials are shown in Table 1. which are collected from experimental and theoretical studies previously published. In the table, N_C and N_V correspond to effective conduction and valence band density, E_g denotes band gap, N_A and N_D denote acceptor and donor density, μ_p (μ_n) represents hole (electron) mobility, N_t is the defect density, χ represents electron affinity and ε_r represents relative permittivity. In this study, the initial defect density of $CsPbI_3$ absorber is assumed as 8×10^{19} cm^{-3}, which gives carrier diffusion length of 1 μm, which is a similar value to the reported work

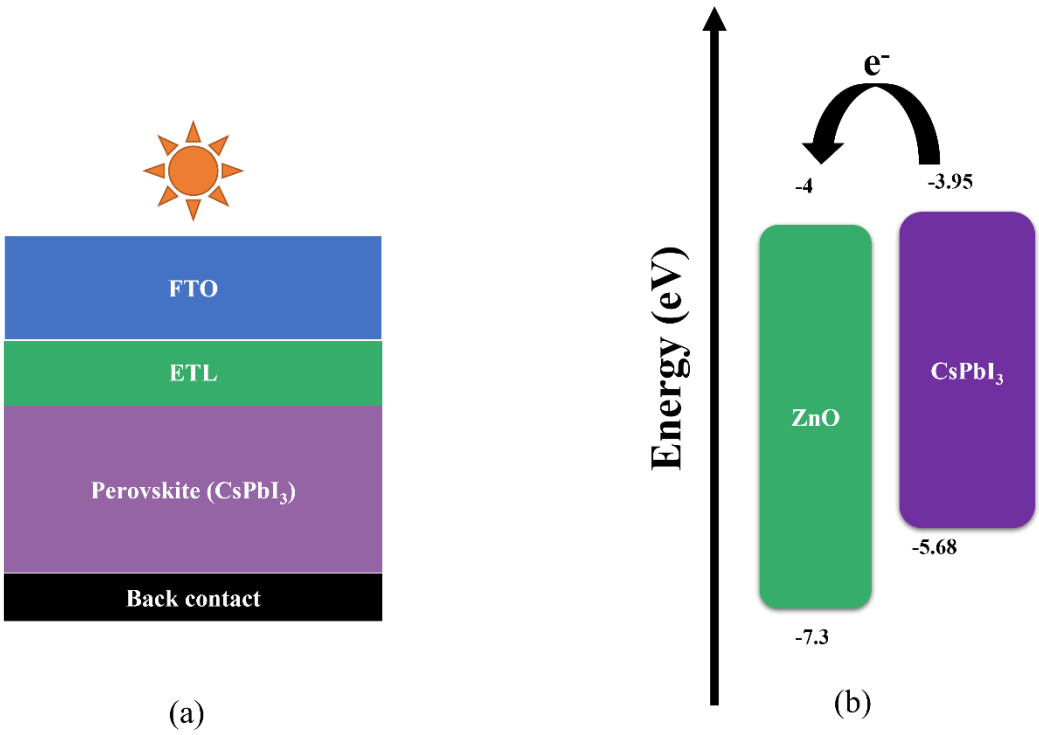

Figure 3(a) The device structure of FTO/ZnO/CsPbI3/Back contact HTL-free solar cell (b) Bandgap alignment of $CsPbI_3$ with ZnO ETL [1] [2]

Table 2 Material parameters for SCAPS simulator

	FTO [29]	**ZnO** [30]	**$CsPbI_3$** [31],[32]
E_g (eV)	3.5	3.3	1.67
χ (eV)	4	4	3.95
ε_r	9	9	4
μ_n ($cm^2/V.S$)	20	100	16
μ_p ($cm^2/V.S$)	10	25	16
N_t (cm^{-3})	10^{15}	10^{15}	2×10^{14}
N_A (cm^{-3})	-	-	10^{15}
N_D (cm^{-3})	10^{18}	10^{18}	-
N_c (cm^{-3})	2.2×10^{18}	2.2×10^{18}	1.1×10^{20}
N_v (cm^{-3})	1.8×10^{19}	1.8×10^{19}	8×10^{19}

3. Results and Discussion

3.1 Verification of the proposed $CsPbI_3$ HTL-free solar cell

To begin the numerical simulation study, a verification of the $CsPbI_3$ HTL free solar cell structure parameters are performed. The proposed solar cell device structure is consisted of FTO/ZnO/$CsPbI_3$/Carbon. Figure 4(a) shows the simulated J-V characteristics diagram. The solar cell parameters simulation values are near the experimental values done by Zhang et al [19] as shown in the embedded table. This structure is used as a reference for the study to further performance evaluation and investigation.

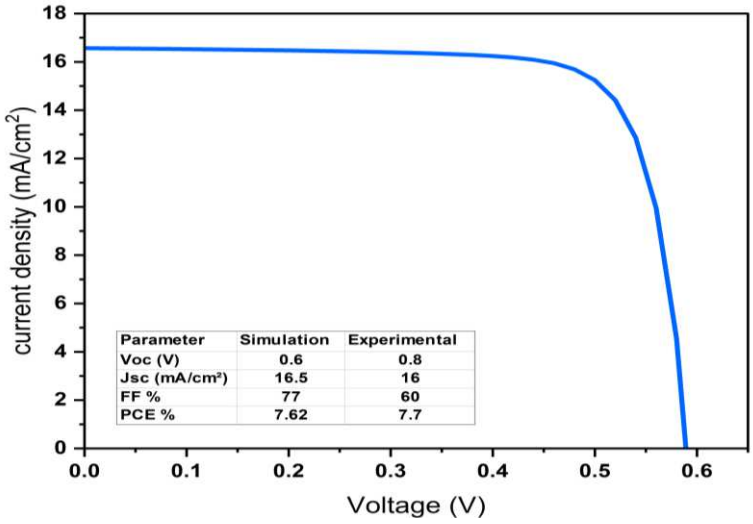

Figure 4 The simulated J-V of FTO/ZnO/$CsPbI_3$/C solar cell structure

3.2 Impact of different metal back contact

Different metals are simulated as back contact to study the performance of solar cell device. The work functions of metals are carbon C (5 eV), gold Au (5.1 eV), platinum Pt (5.65 eV) and selenium Se (5.9 eV). Figure 5 (a) shows the J-V diagram of the solar cell structure with different metals. The Voc values increased with work function increase. A small increase in Voc from 0.6 V for carbon back metal to 0.7 V for using Au as a back metal. Using Pt and Se back metal has a big increase in the Voc values. Selenium has the best solar cell device performance with Voc 1.21 V and considered as an abundant material rather than Au and Pt. Jsc values are close with different metal contact. The PCE values of the solar cell structure with different metal back contacts are shown in figure 5(b). Using C and Au as a back contact has the lowest PCE values, while Pt and Se with higher work function values, the solar cell PCE values are 16% and 17%, respectively. The suggested optimized structure of $CsPbI_3$ HTL free is FTO/ZnO/$CsPbI_3$/Se.

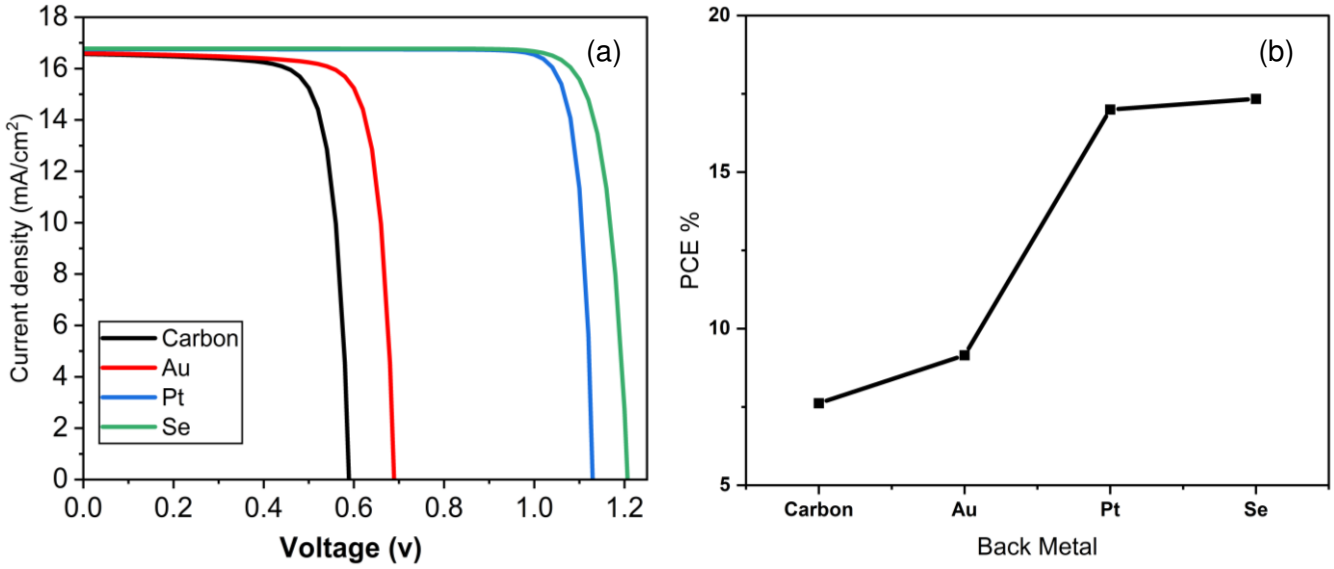

Figure 5 The simulated different back contacts of FTO/ZnO/$CsPbI_3$/back metal solar cell (a) J-V diagram, (b) PCE

3.3 Impact of $CsPbI_3$ thickness

The engineering of perovskite layer thickness has an impact on solar cell device performance. The layer thickness of $CsPbI_3$ is varied from 200 nm to 1000 nm to measure the J-V, quantum efficiency (QE) diagrams and solar cell parameters. Figure 6(a) shows the J-V diagram of FTO/ZnO/$CsPbI_3$/Se structure. The solar cell parameters increase with thickness from 200 to 800 nm. After that, the recombination rate of carriers increases and cause decrease of current density and a slight increase in Voc and PCE values. the QE is shown in figure 6(b). QE values are increased gradually until 800 nm thickness of $CsPbI_3$, which is because of the increased photon absorption. The QE values saturates for thickness larger than 800 nm. The 800 nm thickness of $CsPbI_3$ is the best value of perovskite layer thickness for performance and cost.

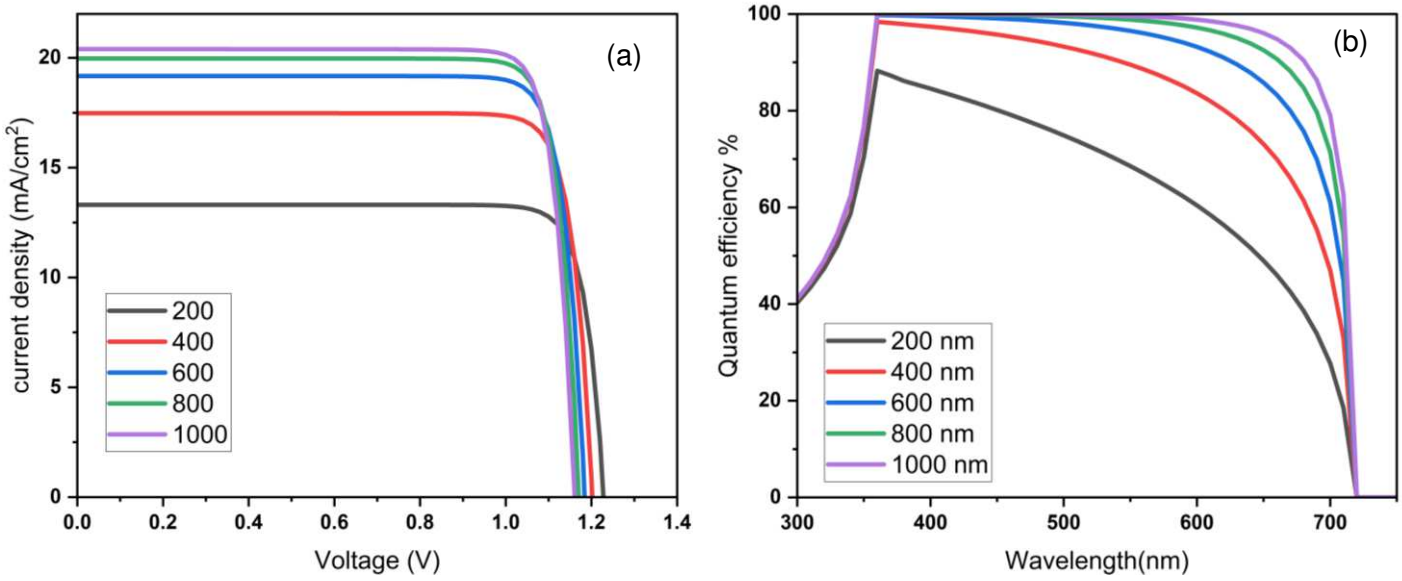

Figure 6 (a) J-V characteristics diagram of FTO/ZnO/CsPbI3/Se, (b) QE with different $CsPbI_3$ thickness

Table 3 solar cell parameters of FTO/ZnO/CsPbI3/Se with different $CsPbI_3$ thickness

Thickness	Voc (Volt)	Jsc (mA/cm^2)	FF %	PCE %
200	1.23	13.3	86	14
400	1.20	17.5	85	18
600	1.18	19	85	19.4
800	1.17	20	86	20.1
1000	1.16	20.4	86	20.3

3.4 Impact of $CsPbI_3$ doping concentration

In the present investigation, the acceptor density (N_A) in $CsPbI_3$ is varied from 10^{15} to 10^{18} cm^{-3}. The J-V curves and PCE with varying N_A are exhibited in Figure 7. As shown, the Jsc values are identical under for acceptor densities from (10^{15} cm^{-3} to 10^{19} cm^{-3}). However, when the N_A is 10^{20} cm^{-3}, the J_{SC} decreases and V_{OC} increases. The Voc values are increased gradually with higher doping N_A. This can be explained as, increasing of N_A produces high electric field across the $CsPbI_3$ material. This allows for the separation and collection of carriers to generate electric field. However, under a high N_A such as10^{20} cm^{-3}, the depleted region became small and the electric field is compressed to the interface between $CsPbI_3$ and ETL. This became as an obstacle to carrier collection and separation and in turns lowers the Jsc value. The increment in Voc can be explained by Equations (1) and (2) as follows

$$I_0 = q\, n_i^2 \left(\frac{D_n}{L_n N_A} + \frac{D_p}{L_p N_D}\right) \qquad (1)$$

$$V_{oc} = \frac{kT}{q} \ln\left(\frac{I_l}{I_0} + 1\right) \qquad (2)$$

Increasing N_A decreases the saturation current I_0 and Jsc. The decrement of I_0 improve the Voc values. The optimum N_A value of the best device performance, As shown in Figure 7(b), a maximum conversion efficiency of 23% can be obtained when N_A is 10^{19} cm^{-3}.

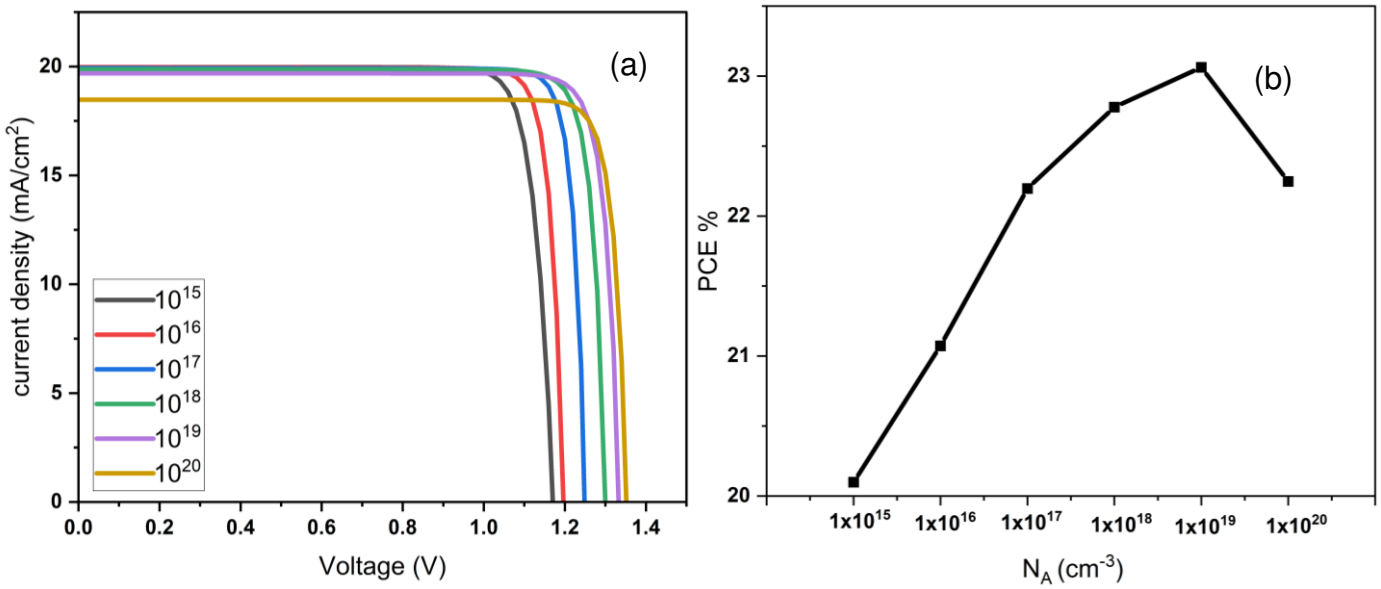

Figure 7 The simulation measurements of FTO/ZnO/$CsPbI_3$/Se solar cell structure with different doping concentration of $CsPbI_3$ (a) J-V, (b) PCE

3.5 Effect of $CsPbI_3$ defect density variation

The impact of absorber defect density N_t is simulated and shown in Figure 8. The J-V characteristic diagram shown in Figure 8 (a). The Nt values has no impact on Jsc but has an impact on Voc values. The decrease of Nt values cause increase of Voc values which affects the PCE of the cell. Figure 8(b) shows the relationship between PCE and different defect densities. As can be seen, when N_t is lower than 2×10^{12} cm^{-3}, the PCE shows few changes. However, when N_t goes beyond 2×10^{15} cm^{-3}, the PCE becomes small. Therefore, controlling the N_t under ~10^{12} cm^{-3} may enhance the PCE of $CsPbI_3$ HTL-free PSCs. At this N_t value, optimized PCE of 23.25% can be achieved for FTO/ZnO/$CsPbI_3$(800 nm)/Se all-inorganic PSCs.

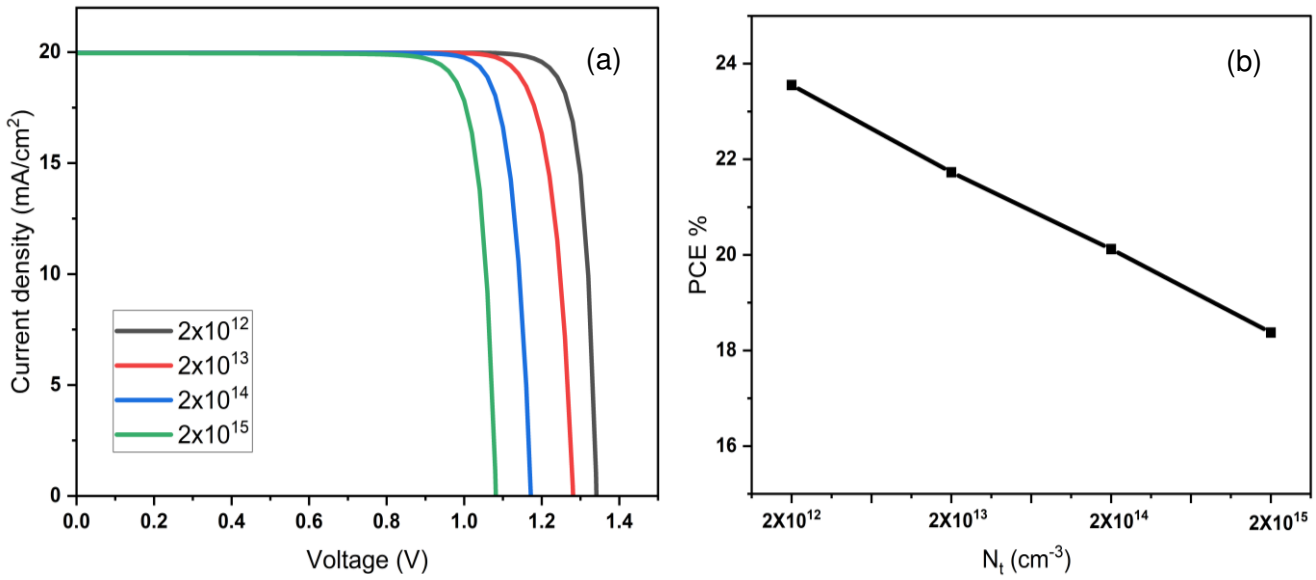

Figure 8 The simulation measurements of FTO/ZnO/$CsPbI_3$/Se solar cell structure with different defect density concentration of $CsPbI_3$ (a) J-V diagram of, (b) PCE

3.6 The simulated optimized structure

The optimized structure of $CsPbI_3$ HTL free based perovskite solar cell can be assumed from the simulation study as: FTO/ZnO/$CsPbI_3$ (800 nm)/Se. The doping acceptor concentration of $CsPbI_3$ layer can be estimated to be 10^{19} cm^{-3} and the best defect density concentration levels N_t of 2×10^{12} cm^{-3}. Figure 9 (a) shows the J-V characteristics diagram of the solar cell. The device short circuit current density (Jsc) of 19.78 mA/cm^2, open circuit voltage (V_{oc}) of 1.34 volts, power conversion efficiency (PCE) of 23.25 % and fill factor (FF) of 87.5%. Figure 9 (b) shows the QE values which are high all over the spectrum.

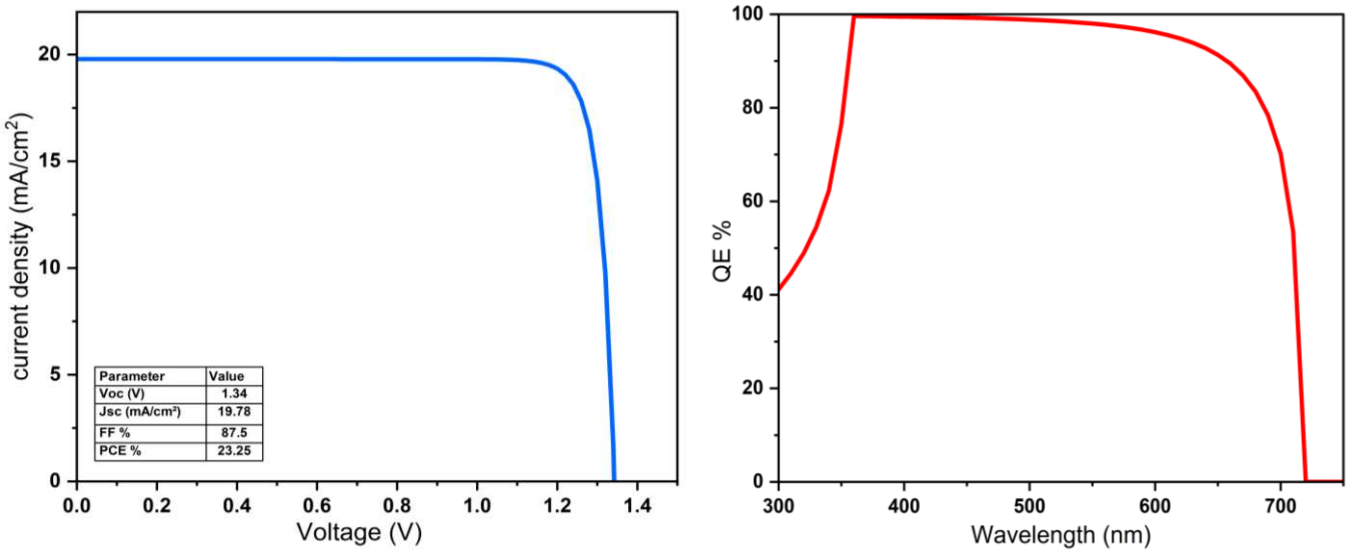

Figure 9 Optimized structure of $CsPbI_3$ hole free perovskite solar cell simulation (a) J-V diagram, (b) QE

Conclusion

In this work, a hybrid DFT and numerical simulation studies are carried on $CsPbI_3$ based perovskite solar cell. The DFT study confirms the experimentally measured optical refractive index. The $CsPbI_3$ material has advantage of minimum reflection of light. The reference simulated solar cell device structure is based on ZnO as an ETL layer and carbon as a back contact. The SCAPS 1D numerical simulator shows that the replacement of metal back contact with low-cost abundant Se gives the device the optimum PCE. The best performance solar cell structure is (FTO/ZnO/$CsPbI_3$/Se) with PCE of 23.25%. The numerical simulation optimization results shows that the optimum thickness of $CsPbI_3$ is 800 nm with acceptor concentration of 10^{19} cm^{-3} and the best defect density concentration is 2×10^{12} cm^{-3}.

References

[1] Unger E L, Kegelmann L, Suchan K, Sörell D, Korte L and Albrecht S 2017 Roadmap and roadblocks for the band gap tunability of metal halide perovskites *J. Mater. Chem. A* **5** 11401–9

[2] Prasanna R, Gold-Parker A, Leijtens T, Conings B, Babayigit A, Boyen H-G, Toney M F and McGehee M D 2017 Band Gap Tuning via Lattice Contraction and Octahedral Tilting in Perovskite Materials for Photovoltaics *J. Am. Chem. Soc.* **139** 11117–24

[3] Sutton R J, Eperon G E, Miranda L, Parrott E S, Kamino B A, Patel J B, Hörantner M T, Johnston M B, Haghighirad A A, Moore D T and Snaith H J 2016 Bandgap-Tunable Cesium Lead Halide Perovskites with High Thermal Stability for Efficient Solar Cells *Adv. Energy Mater.* **6** 1–6

[4] Kojima A, Teshima K, Shirai Y and Miyasaka T 2009 Organometal Halide Perovskites as Visible-Light Sensitizers for Photovoltaic Cells *J. Am. Chem. Soc.* **131** 6050–1

[5] Yin W-J, Shi T and Yan Y 2014 Unusual defect physics in CH3NH3PbI3 perovskite solar cell absorber *Appl. Phys. Lett.* **104** 63903

[6] Juarez-Perez E J, Ono L K, Maeda M, Jiang Y, Hawash Z and Qi Y 2018 Photodecomposition and thermal decomposition in methylammonium halide lead perovskites and inferred design principles to increase photovoltaic device stability *J. Mater. Chem. A* **6** 9604–12

[7] Chen H, Xiang S, Li W, Liu H, Zhu L and Yang S 2018 Inorganic Perovskite Solar Cells: A Rapidly Growing Field *Sol. RRL* **2**

[8] Zhang J, Hodes G, Jin Z and Liu S 2019 All-Inorganic CsPbX3 Perovskite Solar Cells: Progress and Prospects *Angew. Chemie - Int. Ed.* **58** 15596–618

[9] Ahmad W, Khan J, Niu G and Tang J 2017 Inorganic CsPbI3 Perovskite-Based Solar Cells: A Choice for a Tandem Device *Sol. RRL* **1** 1–9

[10] Afsari M, Boochani A and Hantezadeh M 2016 Electronic, optical and elastic properties of cubic perovskite CsPbI3: Using first principles study *Optik (Stuttg).* **127** 11433–43

[11] Yang K, Zhang Y and Lu H 2021 First-principles study on the geometric, electronic and thermodynamic properties of the CsPbI3 (001) surfaces *IOP Conf. Ser. Earth Environ. Sci.* **692**

[12] Singh R K, Kumar R, Jain N, Dash S R, Singh J and Srivastava A 2019 Investigation of optical and dielectric properties of CsPbI 3 inorganic lead iodide perovskite thin film *J. Taiwan Inst. Chem. Eng.* **96** 538–42

[13] Jayan K D, Sebastian V and Kurian J 2021 Simulation and optimization studies on CsPbI3 based inorganic perovskite solar cells *Sol. Energy* **221** 99–108

[14] Hamada K, Yonezawa K, Yamamoto K, Taima T, Hayase S, Ooyagi N, Yamamoto Y and Ohdaira K 2019 Vacuum deposition of CsPbI3 layers on textured Si for Perovskite/Si tandem solar cells *Jpn. J. Appl. Phys.* **58**
[15] Deng W, Li J, Jin J, Mishra D D, Xin J, Lin L, Guo S, Xiao B, Wilson G J and Wang X 2020 Fast and low temperature processed CsPbI3 perovskite solar cells with ZnO as electron transport layer *J. Power Sources* **480** 229134
[16] Tumen-Ulzii G, Qin C, Matsushima T, Leyden M R, Balijipalli U, Klotz D and Adachi C 2020 Understanding the Degradation of Spiro-OMeTAD-Based Perovskite Solar Cells at High Temperature *Sol. RRL* **4** 1–8
[17] Yao X, Liang J, Li Y, Luo J, Shi B, Wei C, Zhang D, Li B, Ding Y, Zhao Y and Zhang X 2017 Hydrogenated TiO2 Thin Film for Accelerating Electron Transport in Highly Efficient Planar Perovskite Solar Cells *Adv. Sci.* **4**
[18] Wan X, Yu Z, Tian W, Huang F, Jin S, Yang X, Cheng Y-B, Hagfeldt A and Sun L 2020 Efficient and stable planar all-inorganic perovskite solar cells based on high-quality CsPbBr3 films with controllable morphology *J. Energy Chem.* **46** 8–15
[19] Zhang J, Wang C, Fu H, Gong L, He H, Fang Z, Zhou C, Chen J, Chao Z and Fan J 2021 Low-temperature preparation achieving 10.95%-efficiency of hole-free and carbon-based all-inorganic CsPbI3 perovskite solar cells *J. Alloys Compd.* **862** 158454
[20] Payne M C, Teter M P, Allan D C, Arias T A and Joannopoulos J D 1992 Iterative minimization techniques for ab initio total-energy calculations: Molecular dynamics and conjugate gradients *Rev. Mod. Phys.* **64** 1045–97
[21] Perdew J P, Chevary J A, Vosko S H, Jackson K A, Pederson M R, Singh D J and Fiolhais C 1992 Atoms, molecules, solids, and surfaces: Applications of the generalized gradient approximation for exchange and correlation *Phys. Rev. B* **46** 6671–87
[22] Trots D M and Myagkota S V 2008 High-temperature structural evolution of caesium and rubidium triiodoplumbates *J. Phys. Chem. Solids* **69** 2520–6
[23] Singh R K, Kumar R, Jain N, Dash S R, Singh J and Srivastava A 2019 Investigation of optical and dielectric properties of CsPbI3 inorganic lead iodide perovskite thin film *J. Taiwan Inst. Chem. Eng.* **96** 538–42
[24] Primak W 1971 Refractive Index of Silicon *Appl. Opt.* **10** 759–63
[25] Sell D D, Casey H C and Wecht K W 1974 Concentration dependence of the refractive index for n - and p -type GaAs between 1.2 and 1.8 eV *J. Appl. Phys.* **45** 2650–7
[26] Park J-S, Choi S, Yan Y, Yang Y, Luther J M, Wei S-H, Parilla P and Zhu K 2015 Electronic Structure and Optical Properties of α-CH3NH3PbBr3 Perovskite Single Crystal *J. Phys. Chem. Lett.* **6** 4304–8
[27] Brittman S and Garnett E C 2016 Measuring n and k at the Microscale in Single Crystals of CH3NH3PbBr3 Perovskite *J. Phys. Chem. C* **120** 616–20
[28] Burgelman M, Decock K, Kheli S and Abass A 2013 Advanced electrical simulation of thin film solar cells *Thin Solid Films* **535** 296–301
[29] Karimi E and Ghorashi S M B 2017 Investigation of the influence of different hole-transporting materials on the performance of perovskite solar cells *Optik (Stuttg).* **130** 650–8
[30] Islam T, Jani R, Amin S M Al, Shorowordi K M, Nishat S S, Kabir A, Taufique M F N, Chowdhury S, Banerjee S and Ahmed S 2020 Simulation studies to quantify the impacts of point defects: An investigation of Cs2AgBiBr6 perovskite solar devices utilizing ZnO and Cu2O as the charge transport layers *Comput. Mater. Sci.* **184** 109865
[31] Dastidar S, Li S, Smolin S Y, Baxter J B and Fafarman A T 2017 Slow Electron–Hole Recombination in Lead Iodide Perovskites Does Not Require a Molecular Dipole *ACS Energy Lett.* **2** 2239–44
[32] Hutter E M and Savenije T J 2018 Thermally Activated Second-Order Recombination Hints toward Indirect Recombination in Fully Inorganic CsPbI3 Perovskites *ACS Energy Lett.* **3** 2068–9